HDL-Mimicking Peptide–Lipid Nanoparticles with Improved Tumor Targeting

Zhihong Zhang, Juan Chen, Lili Ding, Honglin Jin, Jonathan F. Lovell, Ian R. Corbin, Weiguo Cao, Pui-Chi Lo, Mi Yang, Ming-Sound Tsao, Qingming Luo, and Gang Zheng*

Targeted delivery of intracellularly active diagnostics and therapeutics in vivo is a major challenge in cancer nanomedicine. A nanocarrier should possess long circulation time yet be small and stable enough to freely navigate through interstitial space to deliver its cargo to targeted cells. Herein, it is shown that by adding targeting ligands to nanoparticles that mimic high-density lipoprotein (HDL), tumor-targeted sub-30-nm peptide–lipid nanocarriers are created with controllable size, cargo loading, and shielding properties. The size of the nanocarrier is tunable between 10 and 30 nm, which correlates with a payload of 15–100 molecules of fluorescent dye. Ligand-directed nanocarriers targeting epidermal growth factor receptor (EGFR) are confirmed both in vitro and in vivo. The nanocarriers show favorable circulation time, tumor accumulation, and biodistribution with or without the targeting ligand. The EGFR targeting ligand is proved to be essential for the EGFR-mediated tumor cell uptake of the nanocarriers, a prerequisite of intracellular delivery. The results demonstrate that targeted HDL-mimetic nanocarriers are useful delivery vehicles that could open new avenues for the development of clinically viable targeted nanomedicine.

Keywords:
- cancer therapy
- lipids
- nanoparticles
- peptides
- tumor targeting

1. Introduction

Liposomes and polymer nanocarriers are two dominant classes of delivery vehicles for cancer therapeutics and are the only nanocarriers approved for clinical use by the US Food and Drug Administration (FDA).[1–3] However, these nanocarriers have restricted diffusion into solid tumors because their size (>75 nm) is generally larger than the interfibrillar openings (<40 nm)[4] of interstitial collagens at tumor sites. This poses limitations for the delivery of molecular therapeutics (e.g.,

[*] Dr. G. Zheng, Dr. Z. Zhang,[+] Dr. J. Chen,[+] L. Ding, H. Jin,
Dr. I. R. Corbin, Dr. W. Cao, Dr. P.-C. Lo, Dr. M. Yang, Dr. M.-S. Tsao
Department of Medical Biophysics
Ontario Cancer Institute
University of Toronto
TMDT 5-363, 101 College Street, Toronto, ON M5G 1L7 (Canada)
E-mail: gang.zheng@uhnres.utoronto.ca

Dr. Z. Zhang, H. Jin, Dr. Q. Luo
Britton Chance Center for Biomedical Photonics
Wuhan National Laboratory for Optoelectronics
Huazhong University of Science and Technology
Wuhan (China)

Dr. G. Zheng, J. F. Lovell
Institute for Biomaterials and Biomedical Engineering
University of Toronto
Toronto (Canada)

Dr. W. Cao
Department of Chemistry
Shanghai University
Shanghai (China)

[+] These authors contributed equally to this work.

⌨ Supporting Information is available on the WWW under http://www.small-journal.com or from the author.
HDL=high-density lipoprotein.

siRNA, peptides), which modulate intracellular targets rather than target in the tumor microenvironment. Although polymer–lipid micelles can be synthesized below 40 nm,[5,6] they tend to have moderate circulation lifetimes[5] and less stable drug retention than liposomes. While inorganic nanoparticles, such as quantum dots and gold nanoparticles, could be synthesized in this size range, researchers are still optimizing their surface chemistries for in vivo applications and studying their long-term toxicity.[7–10] We postulate that for a nanocarrier to be ideally suited for the delivery of intracellular cancer medicines, it should combine the key advantages of different nanoparticles: the stability and monodispersity of inorganic nanoparticles,[11,12] the sub-40-nm size and drug-loading capacity of polymeric micelles,[5] and the long circulation half-lives and cargo-shielding of liposomes.[1]

Figure 1. A–E) Structure and characterization of the FNC and EGF-FNC and F) the high correlation between the size and cargo payload of the FNC.

High-density lipoprotein (HDL) is an endogenous nanocarrier possessing many of these attractive features.[13] It possesses ultrasmall size control (7–12 nm) through the apoA-1 lipoprotein component and favorable surface properties.[14,15] This unique combination results in long circulation half-lives ranging from 10 to 12 h in rodents and 5 days in humans.[16,17] These half-lives are comparable to those of some of the best-engineered (PEGylated) long-circulating liposomes to date. One potential hurdle in developing HDL as a clinically viable nanocarrier lies in the fact that lipoproteins are isolated from fresh donor plasma, which might result in batch-to-batch variation and pose some scale-up challenges. Thus, a targeted and versatile HDL-mimicking nanocarrier that could freely navigate through interstitial space while protecting its cargo outside the targeted cells would result in better delivery and therapeutic efficacy, and less systemic toxicity of cancer drugs.

Herein, we report the targeting of a new class of sub-30-nm spherical nanostructures, HDL-mimicking peptide–lipid nanoparticles (denoted FNC for fluorescent nanocarrier), which are formed through a self-assembly interaction between a network of amphipathic α-helical peptides,[18] phospholipids, and hydrophobic cargo to mimic nascent HDL. An investigation into the nanostructure's morphology, tumor targeting, cargo loading, and cargo shielding properties is reported.

2. Results

2.1. Nanocarrier Preparation and Characterization

The preparation of the HDL-mimetic nanostructures consisted of two simple steps. First, a lipid emulsion film was formed with 1,2-dimyristoyl-sn-glycero-3-phosphocholine (DMPC), cholesterol oleate (CO), and 1,1′-dioctadecyl-3,3,3′,3′-tetramethylindotricarbocyanine iodide bis-oleate (DiR-BOA).[14] Second, the lipid emulsion film was hydrated with a solution containing a short apoA-1 mimetic peptide (AP) with an amino acid sequence of FAEKFKEAVKDYFAK-
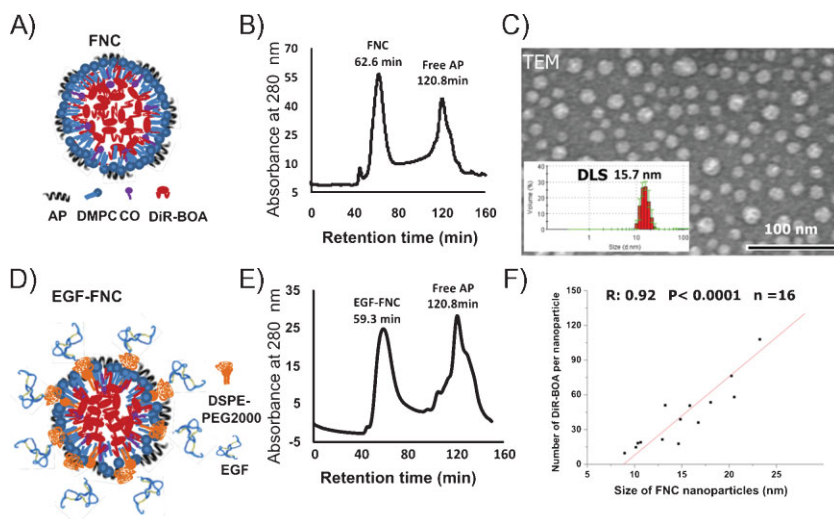
FWD. These steps produced a nanostructure carrying DiR-BOA,[14] a near-infrared fluorescent dye as the model functional cargo, in the core. The structure and characterization of the FNC are shown in Figure 1. The fast protein liquid chromatography (FPLC) profile of the FNC (Figure 1B) showed a well-separated single nanoparticle peak at the retention time of 62.6 min, which enabled easy purification. Zeta potential measurements showed that the FNC surface is mostly neutral (0.087 ± 2.4 mV, $n = 8$). Both dynamic light scattering (DLS) and transmission electron microscopy (TEM; Figure 1C) revealed the size of this spherical FNC to be 15.7 ± 2.9 nm and it is monodispersed. Composition analysis of the FNC showed that the particle contained approximately 50 molecules of DiR-BOA as cargo. Further studies led to the finding that the size of the FNC, between 10 and 30 nm, can be precisely controlled by adjusting the molar ratio of the components in the particle formulation. High correlation between the FNC size and DiR-BOA payload was observed ($R = 0.92$, $P < 0.0001$, $n = 16$; Figure 1F). While smaller particles carried less cargo, the larger 25-nm-sized FNCs carried over 100 DiR-BOA molecules. The FNC also displayed exceptional cargo shielding properties. No leakage of the DiR-BOA cargo was detectable for up to 6 months at 4 °C for FNCs (10–30 nm), and the fluorescence signal in the FNC was stable at 37 °C for 24 h when it was dialyzed in a physiological phosphate-buffered saline (PBS) solution.

To use the FNC to target specific cancer biomarkers, we selected epidermal growth factor receptor (EGFR) as a target and its natural ligand, epidermal growth factor (EGF), as a targeting agent. EGFR is an important cell surface receptor. Along with its ligands, including EGF, it is frequently overexpressed in a variety of solid tumors including cancers of the brain, breast, colon, head and neck, lung, ovary, and pancreas.[19] For the preparation of this targeted FNC, sulfhydryl-containing EGF was conjugated to maleimide-functionalized phospholipids (1.6 mol% DSPE-PEG(2000) maleimide; DSPE = 1,2-distearoyl-sn-glycero-3-phosphoetha-nolamine, PEG = polyethylene glycol) introduced into the

FNC formulation. The resulting nanoparticle is denoted as EGF-FNC, and its structure is depicted in Figure 1D. The FPLC profile of EGF-FNC (Figure 1E) was similar to that of a ligand-free FNC (Figure 1B). A typical EGF conjugation to the FNC particle ($\approx$18 nm) resulted in a conjugation ratio of eight EGF ligands per particle. The DiR-BOA payload of EGF-FNC ($\approx$60 DiR-BOA molecules per $\approx$18 nm EGF-FNC) was also similar to that of FNC. All these data suggest that EGF conjugation did not significantly alter the size or disrupt the integrity of the FNC nanoparticles.

2.2. In vitro Characterization

To investigate the targeting specificity of EGF-FNC to EGFR-overexpressing cells, ldlA7 cells, which normally express very low levels of both EGFR and scavenger receptor class B type I (SR-BI), were transfected with a plasmid encoding an EGFR-green fluorescent protein (GFP) fusion protein. The transfected EGFR-GFP-ldlA7 cells (EGFR[+] and SR-BI[−]) served as EGFR-positive controls while the untransfected ldlA7 cells acted as EGFR-negative controls. As shown in Figure 2, confocal microscopy images demonstrated that cells that expressed GFP (indicating EGFR expression) had significant DiR-BOA uptake (white arrow), whereas cells without any GFP fluorescence (and therefore where no EGFR was expressed) did not display any detectable DiR-BOA uptake (black arrow). This demonstrates that EGF-FNC could specifically deliver its cargo (DiR-BOA) into target cells via EGFR-mediated endocytosis. Furthermore, the same cells were incubated with EGF-FNC and 800-fold excess HDL to test the stability and specificity of EGF-FNC and its ability to escape endosomal trapping (see Figure S1 in the Supporting Information). Confocal images illustrated that there was no change to the specific uptake of EGF-FNC in the presence of HDL competition, which suggests that serum lipoproteins did not disrupt the integrity and targeting of EGF-FNC. Moreover, serial confocal images of the cells obtained at 0.9 μm depths per slice demonstrated that DiR-BOA was released from endosomes over time (Figure S1, Supporting Information). Further evidence was obtained with real-time imaging, which showed that the GFP and DiR-BOA fluorescence signals went from having a high degree of co-localization (yellow) to a low degree of co-localization (as shown in red and green) over a 36-min time interval (Figure S2, Supporting Information).
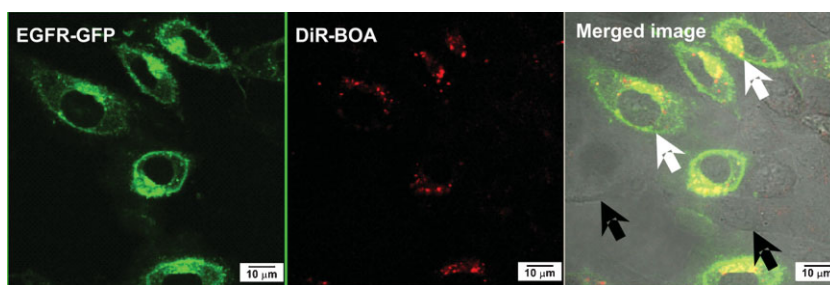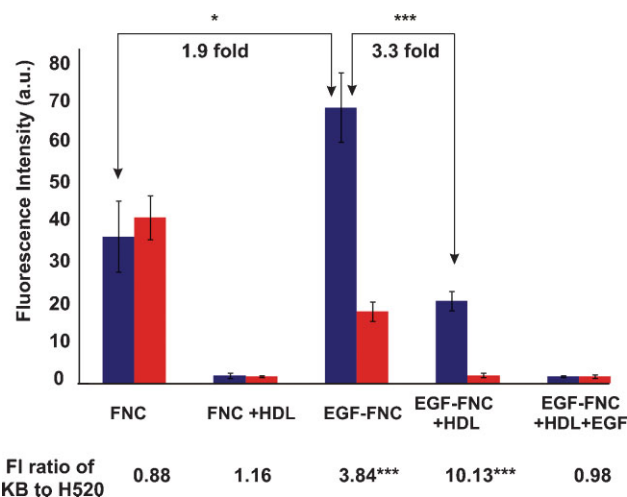

Figure 3. Flow cytometry studies of KB (SR-BI[+], EGFR[+]; blue) and H520 (SR-BI[+], EGFR[−]; red) cells validating the single (EGFR) and dual (EGFR and SRBI) targeting mechanisms. Mean values ± standard deviation, $n = 5$, P values were calculated using nonpaired two-tailed Student's t-test ($^*P < 0.05$, $^{***}P < 0.001$). FI = fluorescence intensity.

After confirming that EGF-FNC could be specifically taken up by EGFR-mediated endocytosis and its contents could be released to the cytosol, we next evaluated the performance of EGF-FNC in EGFR-overexpressing cancer cell lines. KB cells (EGFR[+]) and H520 cells (EGFR[−]) were used as EGFR-positive and -negative controls, respectively (Figure S3, Supporting Information). It should be noted that both KB and H520 cells are positive for SR-BI receptor (SR-BI[+]), which is a natural receptor for HDL[20] and an anticipated target for unmodified apoA-1 mimetic helical peptides.[21] Therefore, it was not surprising that flow cytometry (Figure 3) demonstrated a dual receptor (EGFR and SR-BI) targeting mechanism. It is interesting to note, however, that this targeting mechanism led to a coordinated and enhanced targeting effect in KB cells. The uptake of EGF-FNC by KB cells was 1.9-fold ($n = 3$, $P < 0.05$) greater than the uptake of the untargeted FNC. When excess HDL was used to inhibit SR-BI-mediated uptake, the uptake of EGF-FNC was reduced 3.3-fold in KB cells ($n = 3$, $P < 0.001$). This indicates that the dual receptor-mediated uptake of EGF-FNC in KB cells resulted in an uptake enhancement over the individual receptor-mediated uptake. Compared with the similar FNC uptake in KB and H520 cells, EGF conjugation of FNC resulted in a 1.9-fold increase of EGF-FNC uptake by KB cells but a 2.3-fold ($n = 3$, $P < 0.01$) decrease by H520 cells, presumably because the presence of EGF interfered with SR-BI recognition. As expected, the highest EGFR-targeting specificity was achieved in the presence of HDL inhibition, as evidenced by a 10.13-fold ($n = 3$, $P < 0.001$) difference in EGF-FNC uptake by KB cells versus H520 cells. These observations were consistent with confocal imaging studies (Figure 4), which showed the same uptake/inhibition trends in these two cell lines. Taken

Figure 2. Confocal image studies showed only cells expressing GFP-EGFR (green) with high DiR-BOA (red) uptake (white arrow), whereas EGFR nonexpressing cells did not show any DiR-BOA uptake (black arrow). Scale bar: 10 μm.
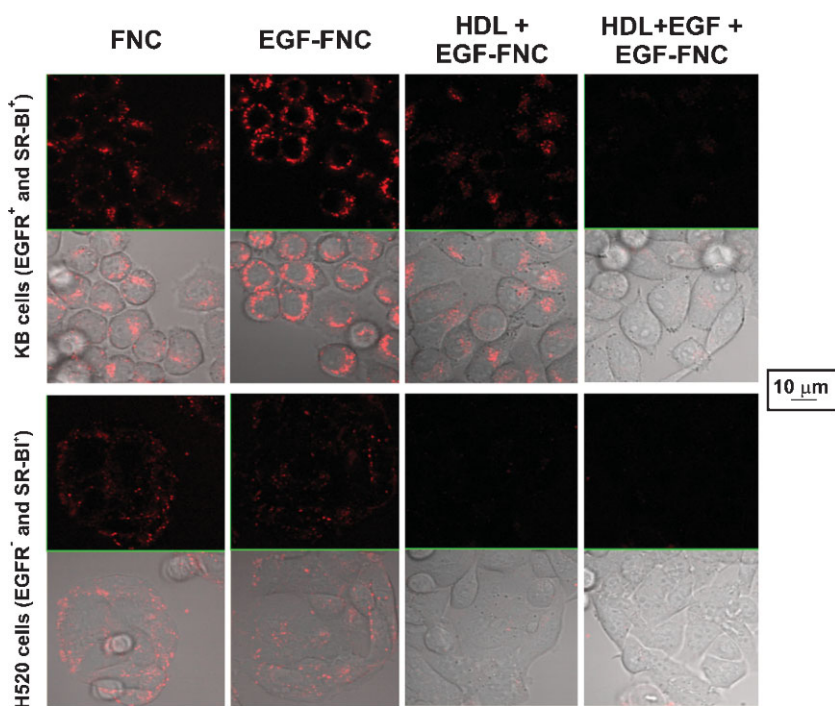
© 2010 Wiley-VCH Verlag GmbH & Co. KGaA, Weinheim

Figure 4. Confocal imaging studies on KB (SR-BI+, EGFR+) and H520 (SR-BI+, EGFR−) cells were consistent with the observations in the flow cytometry studies. KB cells had a higher uptake of EGF-FNC than H520 cells. HDL competition completely blocked the uptake of EGF-FNC in H520 cells but not in KB cells. Only in the presence of both HDL and EGF competition was the uptake of EGF-FNC in KB cells completely blocked. The data support a dual receptor (EGFR and SR-B1)-mediated uptake mechanism for EGF-FNC in KB cells. Scale bar: 10 μm.

together, these data demonstrate that EGF-FNC can be targeted specifically to cancer cells through EGFR, and such targeting can be enhanced by a second targeting pathway (SR-BI).

2.3. In vivo Characterization

The in vivo functional performance of EGF-FNC was assessed. As shown in the blood clearance profiles of EGF-FNC in normal nude mice (Figure 5A), EGF-FNC displayed a long circulation half-life of 13.6 h, which is expected for HDL-like particles in rodents (12–14 h for rats).[16] The long circulation time of EGF-FNC was also evident in the in vivo fluorescence imaging studies, which showed a strong fluorescence signal in the vessel vein at 9 h post-injection (Figure 5A, inset). Next, three groups of nude mice bearing KB tumors on their right flanks were injected intravenously with 1) FNC, 2) EGF-FNC, or 3) EGF-FNC co-administered with HDL. FNC concentrations were adjusted so the same content of DiR-BOA (5 nmol) was injected. As shown in Figure 5B, all three types of FNCs accumulated in the tumor tissues, with the gradual increase of the DiR-BOA fluorescence signal in the tumor beginning at 8 h and peaking at 48 h. This is consistent with the step-by-step process of nanoparticle extravasation, penetration through interstitial space, uptake by tumor cells, and cargo release. Tumors and organs were harvested at 72 h in all three groups (Figure 5C). In all groups, the FNC showed a higher accumulation in the KB tumor (FI per mg) than in other organs (e.g., muscle, heart, lung, kidney, brain), with the

exception of the spleen (equal) and liver (liver:tumor = 4–8-fold, $n = 4$). The moderate spleen uptake of FNC suggests a minimal reticuloendothelial system (RES) uptake that is in agreement with what is observed in native HDL. The fact that all three FNC types with different targeting mechanisms showed similar biodistribution profiles supports an assumption that the size and surface properties play a predominant role in accumulation of the nanoparticles in the tumor tissue.[2,22]

Because EGFR ligand conjugation did not seem to have a major impact on FNC tumor accumulation, we next addressed the question of whether targeting was critical for FNC targeting to tumor cells. For this purpose, two experiments were performed. First, tumor xenografts were generated by KB cells stably expressing mLumin, a far-red fluorescent protein (fRFP) with an absorption peak at 580 nm and emission peak at 620 nm, to provide an intrinsic reference for tumor cells in real time. At 48 h post-injection of EGF-FNC with HDL, both in vivo whole-body images and ex vivo tumor/organ images showed a direct correlation between the cargo (DiR-BOA) signal and tumor cell (fRFP) signal (Figure 6A), which suggests that the EGF-FNC could target tumor cells. A double-tumor-bearing mouse model was introduced with KB (EGFR+ and SR-BI+) on the left flank and H520 (EGFR− and SR-BI+) on the right flank (Figure 6B). Both tumor cells and liver cells were isolated from excised tissues/organs at 48 h post-injection of EGF-FNC with HDL. The fluorescence signals of DiR-BOA extracted from cells were quantified with a spectrofluorometer. The DiR-BOA signal in isolated KB cells was 2.5-fold more than that in isolated H520 cells ($n = 4$, $P < 0.05$), which confirmed the in vivo tumor-cell targeting of EGF-FNC to EGFR (Figure 6B).

Interestingly, we observed a discrepancy of the EGFR-targeting contrast between the in vitro study (tenfold, see Figure 3) and in vivo study (2.5-fold, see Figure 6B). This was most likely due to the fact that tumor blood vessels in both tumor xenografts express EGFR even though tumor cells themselves express very low levels of EGFR.[23,24] It is also worthwhile noting that the ratio of the DiR-BOA signal in liver cells to that in KB cells was only 1.37-fold, which is significantly lower than what was observed in the biodistribution assay (about fourfold, Figure 5C). This may have been because FNC was retained within the liver interstitial space instead of being taken up by the liver cells. Incubation of the EGF-FNC with xenograft tissue slices resulted in cellular uptake of the fluorescent cargo and nuclear exclusion, as determined by confocal microscopy (Figure S5, Supporting Information). Furthermore, the nanocarrier was nontoxic and was well tolerated in a variety of cell lines at lipid concentrations as high as 240 mg mL^{-1} (Figure S6, Supporting Information).
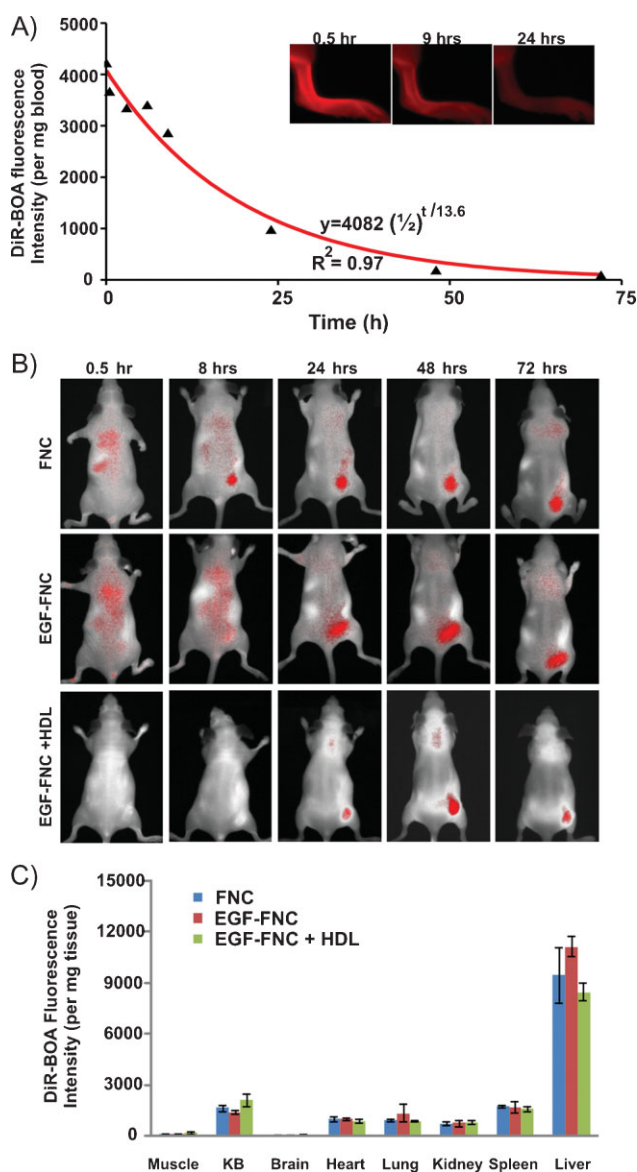
Figure 5. In vivo validation of FNC tumor targeting. A) Blood clearance profiles of EGF-FNC in normal nude mice. The red line represents a data fit to the half-life equation. The data shown are an average of two experiments. Inset: fluorescence image of vessel vein in live mouse. B) In vivo fluorescence imaging of FNC, EGF-FNC, and EGF-FNC with HDL in KB-tumor-bearing mice. Images are shown at five time points: 0.5, 8, 24, 48, and 72 h post-injection. C) Tumor tissue and organ biodistributions at 72 h post-injection of FNC. Mean values ± standard deviation (four mice per group).

Figure 6. In vivo evidence of tumor-cell targeting of FNC. A) Fluorescence imaging of EGF-FNC with HDL in mice bearing KB tumor, which is stably expressing fRFP. The top and bottom rows show DiR-BOA fluorescence (cargos) and fRFP fluorescence (tumor cells), respectively. B) Left: fluorescence imaging of EGF-FNC with HDL in a double KB/H520 tumor-bearing mouse model. Right: relative uptake of DiR-BOA in isolated KB cells, H520 cells, and liver cells at 48 h post-injection of EGF-FNC with HDL. Mean values ± standard deviation, $n = 4$, P values were calculated using nonpaired two-tailed Student's t-test (*$P < 0.05$).

3. Discussion

There has been recent interest in developing synthetic nanosized lipopeptide nanocarriers. Small nanoparticles have been described that are formed from lipids and peptides that target the low-density lipoprotein (LDL) receptor using a fusion peptide containing a LDL receptor-binding and a lipid-binding motif.[25,26] Other small lipopeptide-based nanoparticles have been developed that have proven useful for 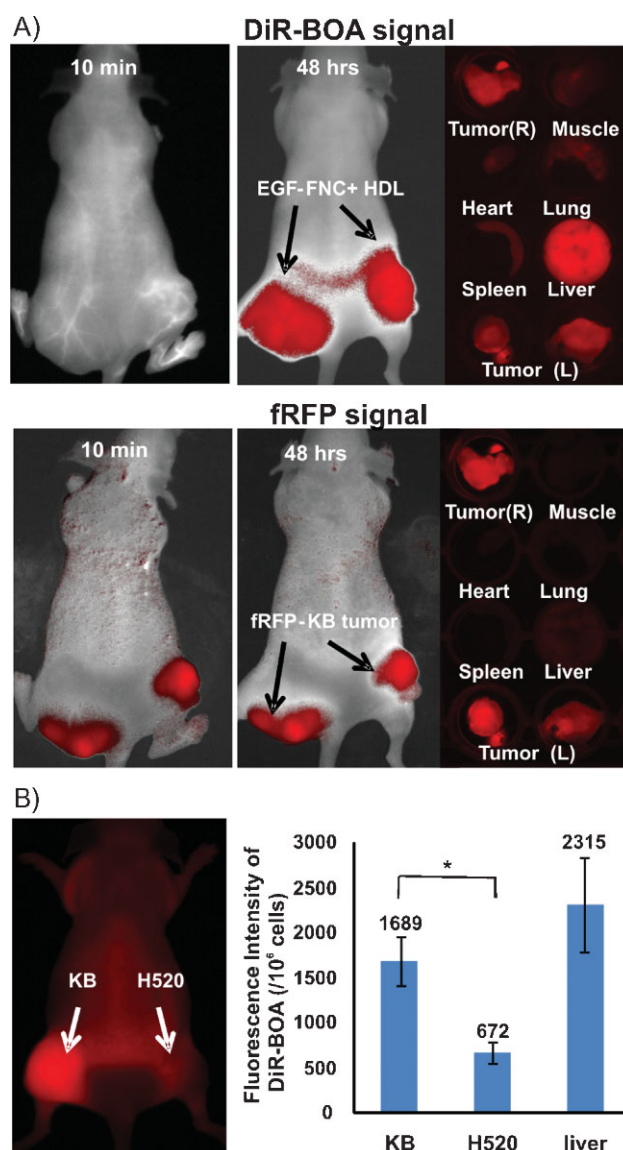DNA delivery.[27] The goal of this study was to build a HDL-mimicking modular nanostructure with optimal surface properties, sub-30 nm in size, and with versatile targeting ability, which could allow the payload-bearing particles to freely navigate through interstitial spaces, thus enhancing both tumor accumulation and access and internalization to tumor cells. Our studies found structural and functional resemblance between FNC and HDL particles. Like HDL particles, FNCs were sub-30-nm, monodisperse, and spherical nanostructures controlled by an amphiphilic α-helical network. However, unlike HDL particles, by varying the amount of cargo, FNCs

showed a high degree of tunability within the 10–30 nm size range. Importantly, the size, shape, and integrity of FNCs were not affected by targeting ligand conjugation. When the FNC was directed to EGFR with EGF ligand conjugation, we observed a coordinated dual receptor (EGFR and SR-BI) targeting phenomenon leading to enhanced cargo delivery. We also found that FNC mimicked the in vivo behavior of HDL.

All FNCs demonstrated favorable tumor accumulation and biodistribution (Figure 5B,C), attributed to the combination of their size and surface properties. In contrast, conventional liposomes are generally in the size range of 75–150 nm and are not stable below 50 nm due to the high lipid curvature required for such sizes. The advantage of using larger liposomes is that the larger size allows for greater loading; however, the larger size may sacrifice tumor penetration. Recent reports[11,28,29] regarding the size effect of nanoparticles seem to be consistent with our observations. It was found that 20-nm particles could permeate the furthest from vessel centers, 60-nm particles less so, and 100-nm particles were restricted to the perivascular region at 8 h post-injection.[29] By comparing the internalization efficiency of gold nanoparticles of different sizes (2, 10, 25, 40, 50, 70 nm), the size dependence of receptor-mediated nanoparticle endocytosis was observed. The most efficient uptake in vivo occurred at 25–50 nm, while the small (2 nm) and large (70 nm) nanoparticles only bound with the surface receptor and could not be internalized.[11] These studies lend support to the potential utility of our sub-30-nm FNC nanoparticles for the intracellular delivery of cancer diagnostics and therapeutics.

The FNC also has several additional features. It is capable of protecting cargo from undesired interactions with plasma proteins. The selective receptor-mediated uptake of FNC cargo (DiR-BOA) by the tumor cells was observed even in the presence of HDL (Figure S1, Supporting Information), serum, or bovine serum albumin (BSA). This feature can reduce the degree of undesirable release of the drug or imaging of cargos before the FNC can reach the target site. Moreover, the method of drug loading can be extended to incorporate a diverse set of diagnostic/therapeutic payloads, given that the payload is suitably hydrophobic. This is particularly useful for payloads requiring extracellular shielding or intracellular delivery. Finally, the methods of ligand conjugation are highly versatile. In addition to the incorporation of targeting ligands through lipid monolayers, like the EGF-FNC validated here, targeting ligands can be conveniently conjugated to the lysine residues of apoA-1 mimetic peptides similar to previously reported LDL rerouting procedures.[30,31] For example, conjugating EGFR-targeted peptide[32] or folic acid[33] to FNCs led to specific FNC targeting to EGFR and folate receptors, respectively (see Figure S4, Supporting Information).

4. Conclusions

In summary, the structural and functional mimicking of HDL provided FNCs with a unique set of physicochemical characteristics, which led to enhanced tumor targeting both in vitro and in vivo. Our studies establish the FNC as a simple, versatile, and biocompatible nanocarrier potentially suitable

for the targeted delivery of clinically relevant cancer diagnostics and therapeutics. Moreover, our results demonstrate that a HDL-mimicking design can improve the in vivo performance of artificial nanomaterials.

5. Experimental Section

Materials: DMPC and DSPE-PEG(2000) maleimide were obtained from Avanti Polar Lipids Inc. (USA). CO and 2-iminotholane hydrochloride (Traut's reagent) were obtained from Sigma–Aldrich Co. (USA). The cell culture media RPMI 1640, Hams F-12, and minimal essential medium (MEM), along with fetal bovine serum (FBS), Geneticin (G418), and trypsin–ethylenediaminetetraacetate (EDTA) solution were all purchased from Gibco–Invitrogen Co. (USA). Human EGF was obtained from R&D Systems, Inc. (USA). The 18 amino acid apoA-1 mimetic peptide (AP), Ac-FAEKFKEAVKDYFAKFWD, was synthesized on a PS-3 peptide synthesizer (Protein Technologies.). DiR-BOA was synthesized by following our previously described procedure.[14] The ldlA7 cell line was kindly provided by Dr. Monty Krieger (Massachusetts Institute of Technology, Cambridge, MA). The human epidermoid carcinoma KB cell line and human lung squamous cell carcinoma H520 cell line were purchased from the American Type Culture Collection.

Preparation of FNC and EGF-FNC: For the preparation of FNCs, a mixture of DMPC (3 μmol), CO (0.1 μmol), and DiR-BOA (0.4 μmol) in chloroform was dried under nitrogen and placed under vacuum for 1 h. PBS buffer (0.1 M, 2 mL, 0.1 M NaCl, pH 7.5) was added to the dried residue and the mixture was vortexed for 5 min. The turbid emulsion was subsequently sonicated for 60 min at 48 °C under nitrogen. AP (0.87 μmol) suspended in PBS buffer (2 mL) was added to the mixture. The turbid emulsion immediately became transparent upon the addition of AP. The resulting heterogeneous complex peptide-associated lipid nanoparticle solution was stored at 4 °C overnight. This complex was then isolated by filtration (0.2 μm) and purified by gel filtration chromatography using the Akta FPLC system (Amersham Biosciences, USA) equipped with a HiLoad 16/60 Superdex 200 pg column. The resulting nanoparticles were eluted with Tris-buffered saline (10 mM Tris–HCl, containing 0.15 M NaCl, 1 mM EDTA, pH 7.5) at a flow rate of 1 mL min^{-1}. The size of the eluted particles was negatively correlated with their respective retention time. FNC particles eluted at a retention time of approximately 60 min and were collected.

For the preparation of EGF-FNC, Traut's reagent (7.26 μmol) was dissolved in Traut's buffer (1 mL; 50 mM triethanolamine, 0.15 M NaCl, 1 mM EDTA, pH 8.0) followed by the addition of EGF (16 nmol). After 1 h of reaction under argon at room temperature, the resulting EGF-SH was collected. The EGF-SH was dialyzed against sodium phosphate buffer (0.1 M, pH 7.5) to remove the excess Traut's reagent. Concurrently, the maleimide-containing FNC was prepared with the same protocol as FNC but with the addition of DSPE-PEG(2000) maleimide at 1.6 mol% of total phospholipid. This FNC was mixed with EGF-SH and shaken at room temperature for 20 h. The resulting EGF-conjugated FNC

(EGF-FNC) was then purified by FPLC. To determine the number of EGF molecules conjugated on each nanoparticle, FNC particles were prepared and separated into two subgroups: one was mixed with EGF-SH and the other served as a negative control. After 20 h, the samples were washed several times with Ultra-4 centrifugal filter devices (30 000 NMWL, Millipore Co.) to remove unconjugated EGF-SH from the EGF-FNC. The concentrations of EGF on the FNC and in the washed solution were determined by using a FluoroProfile protein quantification kit (Sigma–Aldrich Co.). The reported molar ratio of EGF to FNC represents the number of conjugated EGF molecules per FNC nanoparticle.

Morphology, size, and surface charge measurement: TEM was performed using a Hitachi (Japan) H-7000 transmission electron microscope equipped with a digital image acquisition system to determine the morphology and size of an aqueous dispersion of FNC nanoparticles. The particle size distribution and zeta potential of the FNC particles were measured by light-scattering photon correlation spectroscopy (Zetasizer Nano-ZS90; Malvern Instruments, UK) utilizing a 4.0-mW He–Ne laser operating at 633 nm and a detector angle of 90°. For particle size determination, the data were modeled assuming spherical particles undergoing Brownian motion.

Particle composition analysis: determination of C_{AP}: The molar concentration of Ac-FAEKFKEAVKDYFAKFWD (C_{AP}) was determined by quantifying the tryptophan fluorescence at 360 nm. Briefly, FNC was extracted with a mixture of ether/chloroform (7:3), vortexed for 3 min, and then centrifuged at 12 000 rpm for 10 min. The supernatant containing AP was collected and analyzed. The tryptophan residues in the AP were excited at 280 nm and detected at 360 nm using a spectrofluorometer. The C_{AP} was then extrapolated according to a standard curve of AP.

Determination of $C_{DiR-BOA}$: To determine the molar concentration of DiR-BOA ($C_{DiR-BOA}$) in FNC and EGF-FNC solution, the nanoparticle samples were extracted with chloroform, vortexed for 3 min, and then centrifuged at 12 000 rpm for 10 min. The fluorescence intensity of the lower organic layer (containing DiR-BOA) was excited at 748 nm and the fluorescence was detected at 780 nm using a spectrofluorometer. The $C_{DiR-BOA}$ was then determined from a standard curve of DIR-BOA

Determination of C_{DMPC}: The molar concentration of DMPC (C_{DMPC}) of each nanoparticle sample was determined using a Phospholipids C assay kit (Wako Pure Chemical, USA).

Determination of particle composition: The number of DMPC molecules per FNC particle was derived from the published formula, which showed that the number of DMPC molecules in a peptide–lipid discoidal complex can be calculated with the following equation: $2\pi[(d-20)/2]^2/70$.[34] In this equation, assumptions were made that the helix diameter and the surface area/DMPC were 10 Å and 70 Å^2, respectively; d is the diameter of the peptide–lipid complex that is variable. Hence, the number of DMPC molecules in a spherical particle can be approximated from the derived equation $4\pi[(d-20)/2]^2/70$. The molar concentration of FNC nanoparticles (C_{FNC}) was calculated by dividing the concentration of DMPC by the number of DMPC molecules per FNC particle. The number of DiR-BOA molecules per FNC nanoparticle was calculated by dividing $C_{DiR-BOA}$ by C_{FNC}. Similarly, the number of peptide moieties in each FNC nanoparticle was calculated by dividing C_{AP} by C_{FNC}.

In vitro characterization of FNC and EGF-FNC: Cell culture and plasmid transfection: LdlA7, KB, and H520 cells were cultured in Hams F-12, MEM, and RPMI 1640 media, respectively. The transfections of plasmids, pcDNA-EGFR-EGFP (provided by Dr. Peter Verveer, Ludwig Institute for Cancer Research, Royal Melbourne Hospital, Australia) and pCDNA-mLumin, were performed using Lipofectamin 2000 (Invitrogen) according to the manufacturer's protocol. Transfected cells were selected by exposure to Geneticin (800 µg mL^{-1}) and sorted by using flow cytometry with a Becton Dickinson FACS Aria cell sorter for EGFR-GFP-expressing cells and a Dako Cytomation MoFlo nine-color cell sorter for mLumin-expressing cells.

Confocal microscopy and flow cytometry: Cells were seeded into eight-well coverglass-bottom chambers (Nunc Lab-Tek, Sigma–Aldrich; 2×10^4 well^{-1}) for confocal microscopy imaging, and into six-well cell culture plates (3×10^5 well^{-1}) for flow cytometry studies. The cells were incubated with EGF-FNC or FNC at a DiR-BOA concentration of 10 µM for 3 h at 37 °C. For the competition assay, an 800 molar excess of HDL (1 mg mL^{-1}) or 5.6 µM EGF were added. Confocal imaging was performed with an Olympus (Japan) FV1000 laser confocal scanning microscope with excitation wavelengths of 488 nm (exciting GFP) and 633 nm (exciting DiR-BOA). Quantification of the fluorescence signal was achieved using a flow cytometer (Beckman Coulter FC500 five-color analyzer) at an excitation wavelength of 633 nm (exciting DiR-BOA).

In vivo studies of FNC and EGF-FNC: All animal studies were carried out following protocols approved by the Animal Care Committee of the University Health Network.

Blood clearance kinetics: Blood samples were collected from the saphenous vein before and after the intravenous (iv) administration of EGF-FNC nanoparticles at various time points (after 3 min, 30 min, 3 h, 6 h, 9 h, 24 h, and 48 h). The fluorescence intensity of blood samples was measured on a Fluoromax-4 spectrofluorometer and recorded per milligram of blood. A fluorescence intensity versus time plot was used to determine the blood half-life of the nanoparticles.

In vivo near-infrared optical imaging: Three million tumor cells in PBS (0.2 mL) were subcutaneously implanted into the hind flank of mice. Ten to fourteen days following tumor implantation, the tumor-bearing mice received an iv injection of FNC or EGF-FNC (5 nmol DiR-BOA) with or without HDL (containing 1.6 mg protein). In vivo fluorescence images were acquired before injection and 30 min, 8 h, 24 h, 48 h, and 72 h post-injection with a CRI Maestro in vivo imaging system (CRI, USA). Fluorescence images of DiR-BOA were acquired with a deep-red filter set (excitation filter: 671–705 nm; emission filter: 750 nm long pass) and an exposure time of 500 ms. Fluorescence images of mLumin, a far-red fluorescence protein analogue (fRFP),[35] were acquired with a yellow filter set (excitation filter: 575–605 nm; emission filter: 645 nm long pass) and an exposure time of 2000 ms. Following the imaging session the mice were sacrificed and their organs and tumor tissue were excised and imaged.

Biodistribution: Host organs (liver, spleen, heart, muscle, kidney, and brain) and tumor tissue were harvested from mice 48 or 72 h post-injection of FNC or EGF-FNC. Samples were weighed and homogenized in PBS. Homogenates were then extracted by a threefold excess of chloroform/methanol (2:1). The fluorescence

of tissue extracts was measured (excitation: 748 nm; emission: 785 nm) and presented as fluorescence intensity per unit (mg) of tissue. For evaluating in vivo cell uptake of EGF-FNC, the tumor tissue and liver tissue samples were homogenized and filtered with a nylon mesh (pore size 70 μm) to remove debris. The filtered samples (liberated cells) were then washed twice with PBS and treated with red blood cell (RBC) lysis buffer (0.1% potassium bicarbonate, 0.8% ammonium chloride, 0.1 mM EDTA) for 10 min to remove the RBCs. Cells were counted and extracted with chloroform/methanol (2:1). The fluorescence of the cell extract was measured and presented as fluorescence intensity per million cells.

Acknowledgements

[1] T. M. Allen, P. R. Cullis, Science 2004, 303, 1818.
[2] M. E. Davis, Z. G. Chen, D. M. Shin, Nat. Rev. Drug Discovery 2008, 7, 771.
[3] L. Zhang, F. X. Gu, J. M. Chan, A. Z. Wang, R. S. Langer, O. C. Farokhzad, Clin. Pharmacol. Ther. 2008, 83, 761.
[4] A. Pluen, Y. Boucher, S. Ramanujan, T. D. McKee, T. Gohongi, E. di Tomaso, E. B. Brown, Y. Izumi, R. B. Campbell, D. A. Berk, R. K. Jain, Proc. Natl. Acad. Sci. USA 2001, 98, 4628.
[5] V. P. Torchilin, Pharm. Res. 2007, 24, 1.
[6] N. Tang, G. Du, N. Wang, C. Liu, H. Hang, W. Liang, J. Natl. Cancer Inst. 2007, 99, 1004.
[7] E. C. Cho, J. Xie, P. A. Wurm, Y. Xia, Nano Lett. 2009, 9, 1080.
[8] H. S. Choi, W. Liu, P. Misra, E. Tanaka, J. P. Zimmer, B. Itty Ipe, M. G. Bawendi, J. V. Frangioni, Nat. Biotechnol. 2007, 25, 1165.
[9] H. C. Fischer, W. C. Chan, Curr. Opin. Biotechnol. 2007, 18, 565.
[10] H. Wang, X. Chen, Expert Opin. Drug Delivery 2009, 6, 745.
[11] W. Jiang, B. Y. Kim, J. T. Rutka, W. C. Chan, Nat. Nanotechnol. 2008, 3, 145.
[12] X. Gao, Y. Cui, R. M. Levenson, L. W. Chung, S. Nie, Nat. Biotechnol. 2004, 22, 969.
[13] P. C. Rensen, R. L. de Vrueh, J. Kuiper, M. K. Bijsterbosch, E. A. Biessen, T. J. van Berkel, Adv. Drug Delivery Rev. 2001, 47, 251.
[14] I. R. Corbin, J. Chen, W. Cao, H. Li, S. Lund-Katz, G. Zheng, J. Biomed. Nanotechnol. 2007, 3, 367.
[15] J. C. Frias, K. J. Williams, E. A. Fisher, Z. A. Fayad, J. Am. Chem. Soc. 2004, 126, 16316.
[16] S. Eisenberg, H. G. Windmueller, R. I. Levy, J. Lipid Res. 1973, 14, 446.
[17] W. H. Daerr, W. Pethke, E. T. Windler, H. Greten, Biochim. Biophys. Acta 1990, 1043, 311.
[18] L. T. Bloedon, R. Dunbar, D. Duffy, P. Pinell-Salles, R. Norris, B. J. DeGroot, R. Movva, M. Navab, A. M. Fogelman, D. J. Rader, J. Lipid Res. 2008, 49, 1344.
[19] G. Giaccone, Ann. Oncol. 2005, 16, 538.
[20] S. Acton, A. Rigotti, K. T. Landschulz, S. Xu, H. H. Hobbs, M. Krieger, Science 1996, 271, 518.
[21] A. V. Bocharov, I. N. Baranova, T. G. Vishnyakova, A. T. Remaley, G. Csako, F. Thomas, A. P. Patterson, T. L. Eggerman, J. Biol. Chem. 2004, 279, 36072.
[22] D. B. Kirpotin, D. C. Drummond, Y. Shao, M. R. Shalaby, K. Hong, U. B. Nielsen, J. D. Marks, C. C. Benz, J. W. Park, Cancer Res. 2006, 66, 6732.
[23] D. N. Amin, D. R. Bielenberg, E. Lifshits, J. V. Heymach, M. Klagsbrun, Microvasc. Res. 2008, 76, 15.
[24] D. N. Amin, K. Hida, D. R. Bielenberg, M. Klagsbrun, Cancer Res. 2006, 66, 2173.
[25] M. Nikanjam, E. A. Blakely, K. A. Bjornstad, X. Shu, T. F. Budinger, T. M. Forte, Int. J. Pharm. 2007, 328, 86.
[26] I. R. Corbin, G. Zheng, Nanomedicine 2007, 2, 375.
[27] K. Wang, X. Yan, Y. Cui, Q. He, J. Li, Bioconjugate Chem. 2007, 18, 1735.
[28] M. R. Dreher, W. Liu, C. R. Michelich, M. W. Dewhirst, F. Yuan, A. Chilkoti, J. Natl. Cancer Inst. 2006, 98, 335.
[29] S. D. Perrault, C. Walkey, T. Jennings, H. C. Fischer, W. C. Chan, Nano Lett. 2009, 9, 1909.
[30] G. Zheng, J. Chen, H. Li, J. D. Glickson, Proc. Natl. Acad. Sci. USA 2005, 102, 17757.
[31] J. Chen, I. R. Corbin, H. Li, W. Cao, J. D. Glickson, G. Zheng, J. Am. Chem. Soc. 2007, 129, 5798.
[32] Z. Li, R. Zhao, X. Wu, Y. Sun, M. Yao, J. Li, Y. Xu, J. Gu, FASEB J. 2005, 19, 1978.
[33] S. M. Stephenson, P. S. Low, R. J. Lee, Methods Enzymol. 2004, 387, 33.
[34] V. K. Mishra, G. M. Anantharamaiah, J. P. Segrest, M. N. Palgunachari, M. Chaddha, S. W. Sham, N. R. Krishna, J. Biol. Chem. 2006, 281, 6511.
[35] J. Chu, Z. Zhang, Y. Zheng, J. Yang, L. Qin, J. Lu, Z. Huang, S. Zhen, Q. Luo, Biosens. Bioelectron. 2009, 25, 234.